Aix*Marseille université

CENTRALE MARSEILLE

Internship report

Pole expansion of permittivity and optical response of a slab

DIERICK Félice

L3 MPCI November-December 2022

- Supervised by Isam Ben Soltane and Nicolas Bonod -

Contents

Acknowledgements

I would first and foremost like to thank Isam Ben Soltane who is currently doing a PHD in the Clarte team. Even though he was not my official internship supervisor he is really the one I worked with for four weeks. I would like to thank him for making me feel included, useful, and even confident. He had the patience to teach me all sorts of things I had never encountered before while always staying kind and patient. He took the initiative to alter the original subject of my internship to better fill my needs, expectation and capabilities. I was flattered that he allowed me to work on things that are very close to what he was doing, he really made me feel like we were working together. I think that he has definitely left a mark on how I see science; first by the work we did together but also thanks to the discussions we had outside of the main subject, even when taking a break physics was never far from the subject but those discussions really meant a lot to me.
I also cannot forget Nicolas Bonod, the team leader of Clarte and my internship supervisor, who allowed me do this internship. I want to thank him for his generosity but mostly for the validation he gave me for my commitment to my internship. I would also like to thank all the personnel of Fresnel I interacted with, whether they worked in the administration, were researchers, or where working on their PHD. It was a great experience and I feel like I was really included.

Description of the host institution

The Fresnel Institute is a research laboratory that has been conducting research in all sorts of fields surrounding the physics of waves since it's creation in 2000. The research topics are currently divided into 4 main axes: electromagnetic modelling and simulation, nanophotonics and optical components, information processing and random waves and finally advanced imaging and life science. The last of these axis is a more recent one, and thanks to it the lab now also contributes to biophysics and biomedical sciences.
The institue is suported by Aix-Marseille Université, CNRS and Centrale Marseille. It curently has close to 200 people working in it.

The internship was done in the Clarte team led by Nicolas Bonod. The team specialises in electromagnetism, metamaterials aswell as nano and quantum photonics. Isam Ben Soltane the PHD student with whom I worked during my internship is working on meta materials, particularly inverse design for optical components. It often comes down to optimisation problems that try to induce electromagnetic properties through the structuration of simple materials, like metals for example. His work is based around being able to describe the response of a material using only a few particular points called poles in the complex plane. Because the reaction of a material is often dependant on its permittivity, it becomes important to be able to express the permittivity in the complex plane.

The results presented in this report will be part of an article that has yet to be published on the day I sent in this report. I therefore ask the readers not to distribute the contents of this report.

Introduction

Meta materials are materials that are engineered to have properties that are not found in naturally occurring materials. The conception of a meta material requires a good understanding of the behavior of the simpler and more traditional materials that compose it. Among those materials one can often find metals, like gold or silver for example but also many dielectric materials. When conceiving those materials for optical components, the behavior that is often studied is the response of the component to a plane wave. This response is dependent on many characteristics among which we can often find its refractive index and therefore its permittivity. A simple example of the optical components can be optical filters that transmit some frequencies and absorb others. During my internship the goal was to study the response of a metal slab to an incoming wave in the time harmonic domain. I studied work done by Ben Soltane and Colom [11] who derived an expression of the response using a pole expansion method. A Pole expansion is an asymptotic expansions of functions whose terms are of form $a(\omega - p)^{-n}$ where p is a pole of a set function ($p \in \mathbb{C}$), ω is the variable, a is a complex number and n is a positive integer. My contribution was focused around finding a a better model for the refractive index and therefore a model for permittivity in the time harmonic domain on the entire complex frequency plane in order to use it . Historically not many people have studied the expression of the permittivity in the complex frequency plane, though it has become a topic of growing interest thanks to the renewed interest in the theory of resonant states [5, 7]. They also used a pole expansion that they fitted on their data.

I will start by deriving a pole expansion of the permittivity. Then I will present some existing models going from very simple to rather complex and with many parameters ([6, 3]) and how they relate to the experimental data, before comparing one of them to our pole expansion at this point. I will also look at how the pole expansion model relates to experimental data. Finally I will use our model for permittivity to calculate the response of a metal slab to a plane wave.

In order to compare the models for permittivity to experimental data, I used and read about different optimisation algorithms for fitting. This is due to the fact that when a model has been chosen one of the main problems that follows is that of finding the optimal set of parameters to fit the data. For simple models with a small amount of parameters this can be achieved by using Python fitting modules like *curve_fit* from Scipy but for the more complex models I had to use more powerful tools that use more complex criteria for defining what a good fit is. This allows it to find optimal parameters when the standard modules failed.

1 Pole expansion of permittivity

In this document I will be using the following convention for the bilateral Laplace transform of a function f if it exists: $\hat{f}(\omega) = \int_{\mathbb{R}} f(t)e^{i\omega t}dt$. We are talking about a bilateral Laplace transform instead of a Fourier transform because we will be considering $\omega \in \mathbb{C}$.

In this section we will be deriving a pole expansion of permittivity and we will be proving some of its properties.

1.1 Electomagnetic waves

I will start by reviewing Maxwell's equation as they are presented by R.Petit [9] introducing the a relation between the permittivity $\hat{\epsilon}$ and the refractive index n that we will be using to compare our models for $\hat{\epsilon}$ to mesurements made of n. We will be considering that ϵ and μ are scalars, therefore the mediums are isotropic. We will also be supposing that our mediums are homogeneous therefore ϵ and μ are independent of position.

$$\begin{aligned} \nabla \times \mathbf{H} &= \mathbf{J} + \frac{\partial \mathbf{D}}{\partial t}, \\ \nabla \times \mathbf{E} &= -\frac{\partial \mathbf{B}}{\partial t}, \\ \nabla \cdot \mathbf{B} &= 0, \\ \nabla \cdot \mathbf{D} &= \rho. \end{aligned} \tag{1.1}$$

with $\vec{J}$ and ρ the volumic current and charge densities. $\mathbf{E}$ and $\mathbf{D}$ have a linear relation, so do $\mathbf{B}$ and $\mathbf{H}$. It is a convolutive relation in which ϵ and μ act as impulse responses.

$$\mathbf{B} = \mu * \mathbf{H}, \quad \mathbf{D} = \epsilon * \mathbf{E} \tag{1.2}$$

ϵ and μ are respectively the electric permittivity and the magnetic permittivity of the medium. ϵ and μ can be linked to their values in the void by the following relations where n is the refraction index of the medium.

$$\begin{gathered} \epsilon = \epsilon_0 \epsilon_r \text{ and } \mu = \mu_0 \mu_r \\ \hat{\epsilon}_r \hat{\mu}_r = n^2 \end{gathered} \tag{1.3}$$

In the time harmonic domain (1.4) is rewritten as:

$$\begin{aligned} \nabla \times \hat{\mathbf{H}} &= \hat{\mathbf{J}} - i\omega \hat{\mathbf{D}}, \\ \nabla \times \hat{\mathbf{E}} &= i\omega \hat{\mathbf{B}}, \\ \nabla \cdot \hat{\mathbf{B}} &= 0, \\ \nabla \cdot \hat{\mathbf{D}} &= \hat{\rho}. \end{aligned} \tag{1.4}$$

This is due to the fact that the bilateral Laplace transform is linear and because using an integration by parts, if the following integral converges we have:

$$\widehat{\left(\frac{\partial f}{\partial t}\right)}(\omega) = \int_{\mathbb{R}} \frac{\partial f}{\partial t}(t)e^{i\omega t}dt = -\int_{\mathbb{R}} f(t)i\omega e^{i\omega t} = -i\omega \hat{f}(\omega) \tag{1.5}$$

Where f is so that $\lim_{|t|\to\infty} f(t) = 0$.

We can also show using integration by substitution, that for f, g function of time $\widehat{f * g}(\omega) = \hat{f}(\omega)\hat{g}(\omega)$. Therefore we can rewrite (1.2) as:

$$\hat{\mathbf{B}} = \hat{\mu}\hat{\mathbf{H}}, \quad \hat{\mathbf{D}} = \hat{\epsilon}\hat{\mathbf{E}} \tag{1.6}$$

For the expression of the refraction index we will be working under the hypothesis that $\hat{\mu}_r = 1$ therefore $\hat{\epsilon}_r = n^2$.

1.2 Physical properties for $\hat{\epsilon}$

In this section we will be using physical properties of waves to deduce the signs of the real and imaginary parts of n. those signs will then give us the sign of the imaginary part of $\hat{\epsilon}$ on the real axis. This will allow us to later on give more constrains to our fitting algorithm that looks for the optimal set of parameters to model $\hat{\epsilon}$.
Using Maxwell's equations from section 1.1, and in the time and space harmonic domain we can derive a relation between k the wave number and ω.

$$k^2 = \frac{n^2\omega^2}{c^2} \tag{1.7}$$

We will also be considering our signal only propagates along the z axis. We can now express the Electric field $\mathbf{E}$ as the following inverse Laplace transform

$$\mathbf{E}(t,z) = \frac{1}{2\pi}\int_{-\infty}^{+\infty} \hat{\mathbf{E}}(\omega)e^{i(n\frac{\omega}{c}z-\omega t)}d\omega \tag{1.8}$$

Lets now consider a single plane wave that is expressed as $\mathbf{E}_0 e^{i(n\frac{\omega}{c}z-\omega t)}$ with $\omega \in \mathbb{R}$ and $\mathbf{E}_0 \in \mathbb{C}$. If the imaginary part of n is negative, the plane waves diverges as it propagates through space. This would mean that the Electric field $\mathbf{E}$ has infinite energy, This is of course impossible, we can therefore conclude that for $\omega \in \mathbb{R}_+$ $Im(n(\omega)) \geq 0$. We are also considering waves that propagate trough one or multiple mediums but we are not considering counter propagating wave therefore $Re(n(\omega)) \geq 0$.

In order to find conditions on the real and imaginary parts of $\hat{\epsilon}$ we will start by rewriting the relation between $\hat{\epsilon}_r$ and n given in 1.3. For $n = n_r + in_i$, $n_r, n_i \in \mathbb{R}_+$ we can express the permittivity as:

$$\hat{\epsilon} = \epsilon_0\hat{\epsilon}_r = \epsilon_0 n^2 = \epsilon_0(n_r^2 - n_i^2 + 2in_r n_i). \tag{1.9}$$

We can finally deduce that $Im(\hat{\epsilon}) \geq 0$ because n_r and n_i have the same sign.

1.3 Deriving a model for $\hat{\epsilon}$

During the first week of my internship I was guided to demonstrate that we can write $\hat{\epsilon}$ as a pole expansion. I generalised a couple of results and mostly focused on understanding results from Ben Soltan [10]. Some of the expressions I worked on, like the factored form around a point that is not 0, will not be presented in this report since they did not prove themselves usefull to the final project. From this point on when we will talk about ϵ it actualy describes ϵ_r since that is the actual quantity we are interested in to study n.

In this section I will be deriving the pole expansion of the permittivity $\hat{\epsilon}$. We will be considering that ϵ is causal therefore $\epsilon(t) = u(t)\epsilon(t)$ with u that is the Heaviside step function. We will also be considering $\hat{\epsilon}$ is a meromorphic function, therefore it can be expressed as its Taylor series at any point on the complex plane except on a discrete amount of poles at which it can be expressed as a Laurent series

Notation: We will be writing the Laurent series of $\hat{\epsilon}$

$$\hat{\epsilon}(w) = \sum_{n=0}^{+\infty} \frac{\alpha\,(p,n)}{(\omega-p)^n} + \sum_{k=1}^{+\infty} \beta(p,k)(\omega-p)^n \tag{1.10}$$

.

We therefore have the residue of $\hat{\epsilon}$ at p is $Res(\hat{\epsilon}, p) = \alpha(p, 1)$. In order to derive the pole expansion of $\hat{\epsilon}$ we will need the following properties:
Property: The residue of a meromorphic function f at $p \in \mathbb{C}$ is equal to $\frac{1}{2i\pi}$ times the integral for f on a closed contour containing no singularities except p.

Since i did not use this property in any of my classes I will give a proof since it is fundamental to the pole expansion. Let γ be a contour containing no singularities excepts p. We can, thanks to Cauchy's integral theorem, assume that $\gamma = \{z \in \mathbb{C}, |z - p|h\}$ with $h > 0$ and h small enough so that there are no singularities except p. By writing f as its Laurent series we have

$$\oint_\gamma f(\omega)d\omega = \oint_\gamma \sum_{n=0}^{+\infty} \frac{\alpha\left(f, p, n\right)}{(\omega - p)^n} + \sum_{k=1}^{+\infty} \beta(f, p, k)(\omega - p)^n d\omega \tag{1.11}$$

Since $f \in L_1(\gamma)$ because it is holomorphic, we can invert the series and the integral. When calculating the residue associated to a single term in the sum we find have:

$$\oint_\gamma \frac{1}{(\omega - p)^n} d\omega = \begin{cases} 2i\pi, & \text{if } n = 1 \\ 0, & \text{if } n \neq 1 \end{cases} \tag{1.12}$$

Therefore

$$\oint_\gamma f(\omega)d\omega = 2i\pi\alpha(f, p, 1) = 2i\pi Res(f, p) \tag{1.13}$$

Theorem (Cauchy's residue theorem): The integral on a closed contour γ of a meromorphic function f is equal to $2i\pi \sum_{p \in P} Res(f, p)$ where P is the set of all singularities of f contained inside γ.

Let's consider a circular domain of radius $R \in \mathbb{R}$ $A = \{z \in \mathbb{C}, |z| \leq R\}$, it's contour γ and a complex number ω which is not a singularity of $\hat{\epsilon}$. Using Cauchy's Residue theorem we find that

$$\int_\gamma \frac{\hat{\epsilon}(z)}{z - \omega} dz = 2i\pi \sum_{p \in P} Res\left(\frac{\hat{\epsilon}(z)}{z - \omega}, p\right) \tag{1.14}$$

Where $P = \{z \in A, z \text{ is a singularity of } x \mapsto \frac{\hat{\epsilon}(x)}{x - \omega}\}$
Since ω is not a singularity of $\hat{\epsilon}$ we find that $Res\left(\frac{\hat{\epsilon}(z)}{z - \omega}, \omega\right) = \hat{\epsilon}(\omega)$. In order to calculate the residue on a singularity $p \neq \omega$ we first have to calculate the Laurent series at p of $z \mapsto \frac{\hat{\epsilon}(z)}{z - \omega}$ Around p, $z \mapsto \frac{1}{z - \omega}$ is holomorphic and its Taylor series is $\sum_{k=0}^{\infty} -\frac{(z-p)^k}{(p-\omega)^{k+1}}$. By multipling that Taylor series with the Laurent series of $\hat{\epsilon}$ and supposing p is a pole of order ν_p we find

$$Res\left(\frac{\hat{\epsilon}(z)}{z - \omega}, p\right) = \sum_{n=0}^{\nu_p} -\frac{\alpha\left(p, n\right)}{(\omega - p)^n} \tag{1.15}$$

We can now rewrite (1.14) as

$$\int_\gamma \frac{\hat{\epsilon}(z)}{z - \omega} dz = 2i\pi\hat{\epsilon}(\omega) - 2i\pi \sum_{p \in P} \sum_{n=1}^{\nu_p} \frac{\alpha\left(p, n\right)}{(\omega - p)^n} \tag{1.16}$$

where P is the set of poles of $\hat{\epsilon}$ contained in A.

By using (1.16) on a point $a \in A$ that is not a singularity for $\hat{\epsilon}$, we have

$$\int_\gamma \frac{\hat{\epsilon}(z)}{z-a}dz = 2i\pi\hat{\epsilon}(a) + 2i\pi \sum_{p\in P}\sum_{n=0}^{\nu_p} -\frac{\alpha\,(p,n)}{(a-p)^n} \tag{1.17}$$

In order to have an approximate expression of $\hat{\epsilon}(\omega)$ using the information of $\hat{\epsilon}$ on its poles and its value at a we would want the integrals from (1.16) and (1.17) to be equal. This approximation can be justified if we take a the radius R of γ tends to infinity and $\lim_{z\to\infty}\left|\frac{\hat{\epsilon}(z)}{z}\right| = 0$.
We introduce $\hat{\epsilon}_0 = \max_{z\in\gamma}(|\hat{\epsilon}(z)|)$.

$$\begin{aligned}\left|\int_\gamma \frac{\hat{\epsilon}(z)}{z-\omega}dz - \int_\gamma \frac{\hat{\epsilon}(z)}{z-a}dz\right| &= \left|\int_\gamma \frac{(\omega-a)\hat{\epsilon}(z)}{(z-\omega)(z-a)}dz\right| \leq |w-a|\left|\int_{\theta=0}^{2\pi}\frac{R\hat{\epsilon}_0}{(Re^{i\theta}-\omega)(Re^{i\theta}-a)}\right| \\ &\leq |w-a|\frac{\hat{\epsilon}_0}{R}\left|\int_{\theta=0}^{2\pi}\frac{1}{(e^{i\theta}-\frac{\omega}{R})(e^{i\theta}-\frac{a}{R})}\right| = O_\infty\left(\frac{\hat{\epsilon}_0}{R}\right)\underset{R\to\infty}{\longrightarrow} 0\end{aligned} \tag{1.18}$$

Let's now now suppose that $\lim_{z\to\infty}\left|\frac{\hat{\epsilon}(z)}{z}\right| = 0$, we can now write:

$$\hat{\epsilon}(\omega) \approx \hat{\epsilon}(a) - \sum_{p\in P}\sum_{n=0}^{\nu_p}\frac{\alpha\,(p,n)}{(a-p)^n} + \sum_{p\in P}\sum_{n=0}^{\nu_p}\frac{\alpha\,(p,n)}{(\omega-p)^n} \tag{1.19}$$

If we consider that γ has a radius of $R=\infty$ (1.19) becomes an equality. The residual part of $\hat{\epsilon}$ is defined as $\hat{\epsilon}_{res} = \hat{\epsilon}(a) - \sum_{p\in P}\sum_{n=0}^{\nu_p}\frac{\alpha(p,n)}{(a-p)^n}$, it corresponds to the part of $\hat{\epsilon}(\omega)$ that is independent of ω. When $R=\infty$ which is equivalent to when we are considering all the poles of $\hat{\epsilon}$ we have:

$$\hat{\epsilon}(\omega) = \hat{\epsilon}_{res} + \sum_{p\in P}\sum_{n=0}^{\nu_p}\frac{\alpha\,(p,n)}{(\omega-p)^n} \tag{1.20}$$

The condition for this pole expansion to be valid is when $\lim_{z\to\infty}\left|\frac{\hat{\epsilon}(z)}{z}\right| = 0$. In all of the existing models for permittivity we encountered, whether their purpose was to be used in the complex plane [4], or on the real axis [3, 6], it converges when $\omega\to\infty$ thus we can assume that the condition generally holds. In practice, for functions corresponding to physical quantities, only poles of order 1 are considered in most articles. This is due to the fact that it is very difficult to sample the function's value outside of the real axis, therefore we can not estimate the order of the poles. Using only poles of order one is often precise enough to fit data well. We will therefore be expressing $\hat{\epsilon}$ with poles of order one only

$$\hat{\epsilon}(\omega) = \hat{\epsilon}_{res} + \sum_{p\in P}\frac{\alpha\,(p,1)}{(\omega-p)} \tag{1.21}$$

We can note that any meromorphic function that does not diverge faster than the identity can be expressed using this pole expansion [10].

1.4 Pole distribution and time domain

Now that we have a general expression of the pole expansion of $\hat{\epsilon}$ we can use properties of ϵ in the time domain in order to deduce properties of $\hat{\epsilon}$ its expression in the harmonic domain.

In this section we will use the fact that ϵ is a real function and the hypothesis that it does not diverge as $t\to\infty$, to derive properties that are imposed on the pole expansion for it to correctly

model $\hat{\epsilon}$. We start by showing that for any pole p of $\hat{\epsilon}$ with a residue α, $-p^*$ is also a pole of $\hat{\epsilon}$ and the associated residue is $-\alpha^*$.
Let's now consider a pole p of $\hat{\epsilon}$. We have $\lim_{h\to 0}(h)\hat{\epsilon}(p+h) = \alpha$. Since $\hat{\epsilon}$ is the bilateral Laplace transform of a real function it has hermitian symmetry, $\hat{\epsilon}(-\omega^*) = \hat{\epsilon}(\omega)^*$. For any $h \in \mathbb{C}$:

$$-h^*\hat{\epsilon}(-p^* - h^*) = -h * \hat{\epsilon}(p+h)^* \tag{1.22}$$

Since taking the complex conjugate is a continuous operation:

$$lim_{h\to 0} - h^*\hat{\epsilon}(-p^* - h^*) = lim_{h\to 0} - h^*\hat{\epsilon}(p+h)^* = -\left(lim_{h\to 0} - h\hat{\epsilon}(p+h)\right)^* = -\alpha^* \tag{1.23}$$

When considering a pole p with an associated residue (the numerator of the fraction corresponding to the pole in its pole expansion) α of order $n > 0$,We have shown in a similar manner that $-p^*$ would still be a pole but the associated residue would become $(-1)^n\alpha^*$. In our case we can remember the result for poles of order one.

An interesting property that we can note is that the residues associated to poles of order 1 that is located on the imaginary axis has to be imaginary. Let's consider a pole p on the imaginary axis and its associated residue α. Since $p = -p^*$ and the residue associated to $-p^*$ is $-\alpha^*$ we find $-\alpha^* = \alpha$. Therefore $Re(\alpha) = 0$. This condition is a restriction we will later on have to account for when fitting our model on experimental data.
By using the expression of ϵ in the time domain we can also restrict the positions of the poles of $\hat{\epsilon}$ to the bottom half of the complex plane. Using the condition found in the section above we can rewrite $\hat{\epsilon}$ as:

$$\hat{\epsilon}(\omega) = \hat{\epsilon}_{res} + \sum_{p_i \in P_i} \frac{\alpha_{p_i}}{\omega - p_i} + \sum_{p \in P} \frac{\alpha_p}{\omega - p} - \frac{\alpha_p^*}{\omega + p^*} \tag{1.24}$$

Where P is the set of poles of $\hat{\epsilon}$ with a positive real part and P_i is the set of imaginary poles. We do not have to consider poles with negative real parts since they correspond to the hermitian conjugates of those that have positive real parts.
Since $\epsilon(t)$ is causal its bilateral Laplace transform is actually just the usual Laplace transform. Lets consider $f : t \mapsto -iu(t)e^{-i\omega_0 t}$,it's Laplace transform is $\hat{f} : \omega \mapsto \frac{1}{\omega - \omega_0}$. We can use this result along with the linearity of the transform to calculate $\epsilon(t)$ using (1.24). We can easily deduce that the poles on the imaginary axis have to be in the bottom half of the complex plane, if one of them was on the top half ϵ would diverge exponentially. For the remaining poles, one could imagine that signals of identical frequency could compensate each other, therefore we will look at the inverse transform of $\hat{g} : \omega \mapsto \frac{\alpha_p}{\omega - p} - \frac{\alpha_p^*}{\omega + p^*}$ with $p = p_r + ip_i$ and $\alpha = \alpha_r + i\alpha_i$ both complex numbers.

$$g(t) = -iu(t)\left(\alpha e^{-ipt} - \alpha^* e^{ip^*}\right) = -iu(t)e^{p_i t}\left(\alpha_r(e^{-ip_r t} - e^{ip_r t}) - i\alpha_i(e^{-ip_r t} + e^{ip_r t})\right) \tag{1.25}$$

By recognising the sine and cosine functions we notice that g is in fact a real function and that it diverges exponentially if $p_i > 0$. Therefore we can conclude that the poles of $\hat{\epsilon}$ are all located in the bottom half of the complex plane. This again will be accounted for when fitting experimental data.

2 Existing Models for permittivity

In this section we will start by deriving the Drude Lorentz model before using different forms of it to fit our experimental data. We will then compare the existing models with our pole expansion.

2.1 Deriving the Drude Lorentz model

In this section we will be deriving the Drude-Lorentz model for permittivity, then we will study the different simplifications we can do and the domains on which they are valid before finally comparing it to an expression obtained by using the pole expansion method. The Drude Lorentz model is a very common model for permittivity on the real axis. It considers electrons as punctual particles of mass m that can move. We will be considering a material of electric susceptibility χ. In this material we will consider that the electrons are subjected to an electric force pulling them towards the center of the atom as well as a viscous force that acts as a damping force and the Lorentz force generated by the electric field $\mathbf{E}$. Using newtons second law on a single electron we have:

$$m\left(\partial_t^2\mathbf{r} + \partial_t\gamma\mathbf{r} + \omega_0^2\mathbf{r}\right) = -e\mathbf{E}. \tag{2.1}$$

In the time harmonic domain (2.1) gives the following expression for $\mathbf{r}$.

$$\mathbf{r} = -\frac{e}{m\left(\omega_0^2 - i\gamma\omega - \omega^2\right)}\mathbf{E} \tag{2.2}$$

resulting in the expression a the dipole moment $\mathbf{p}$ being:

$$\mathbf{p} = -e\mathbf{r} = -\frac{e^2}{m}\frac{1}{\omega^2 + i\gamma\omega - \omega_0^2}\mathbf{E}. \tag{2.3}$$

Let N be the molecule density of the material. For each molecule we will divide its electrons into groups of n_i electrons that have the same behavior. We will also suppose:

$$\mathbf{P} = \epsilon_0\chi\mathbf{E}. \tag{2.4}$$

Where P is the polarisation of the medium. Therefore we have $\hat{\epsilon}_r = 1+\chi$ According to Jackson[6], we can express the electric susceptibility χ as the sum of the dipole moments of all the electrons in a unit of volume to finally obtain:

$$\hat{\epsilon}_r(\omega) = 1 - \frac{Ne^2}{m}\sum_i \frac{n_i}{\omega^2 + i\gamma\omega - \omega_i^2}. \tag{2.5}$$

This result corresponds to what we can find in the literature (for example [6]). In order to obtain a model with a bit more freedom we usually encounter it under this form

$$\hat{\epsilon}(\omega) = \epsilon_\infty - \sum_i \frac{s_i\omega_i^2}{\omega^2 + i\gamma\omega - \omega_i^2}. \tag{2.6}$$

Where $\epsilon_\infty \in \mathbb{C}$ is the permittivity for very high frequencies. The last statements holds true under the condition that $\hat{\epsilon}$ has a finite amount of poles it would also hold true if when $\lim_{|\omega|\to\infty} |\omega - p_\omega| = 0$, for $\omega \in \mathbb{R}$ where p_ω is the closest pole to ω under the condition that the pole density does not increase too fast when $|Re(\omega)| \to +\infty$.

2.2 Single Pole Drude model

The simplest approximation for (2.6) would be when seeking an equivalent when $\omega \to \infty$. We can then express it as follows:

$$\hat{\epsilon} = \epsilon_\infty - \left(\frac{\omega_p}{\omega}\right)^2 \quad \omega_p \in \mathbb{R}. \tag{2.7}$$

We will call this model the single pole Drude model. According to Smith[2] this model works best for very high frequencies. [6] also mentions it is best suited for modeling materials with

a very low density like plasma for example. Our primary interest is the permittivity of metals therefore we can already say this model will not fit our data. The simplicity of this model has to be mentioned. This model only has two parameters and only returns real values when given a real frequency. This enforces the idea that it is not able to model a real material like gold very well. We notice that 0 is a pole of order 2 for $\hat{\epsilon}$ which is impossible due to physical considerations. We can show that if 0 is a pole of $\hat{\epsilon}$ it has to be of order 1.
Since ϵ is an impulse response for a convolutive system, we can characterise it as the response to a dirac distribution. If we take $\mathbf{E} = \delta(\mathbf{e}_x + \mathbf{e}_y + \mathbf{e}_z)$, with δ being the dirac distribution, we find that the associated displacement field $\mathbf{D} = \epsilon(t)(\mathbf{e}_x + \mathbf{e}_y + \mathbf{e}_z)$. After an infinite amount of time the material returns to a state of equilibrium. This can be its original state or one that has been altered. Therefore $\lim_{t\to\infty} \mathbf{D}(t) = \mathbf{c_0} \in \mathbb{R}^3$

$$\lim_{t\to\infty} \epsilon(t) = c \in \mathbb{R} \tag{2.8}$$

Using the final value theorem we have:

$$c = \lim_{t\to\infty} \epsilon(t) = \lim_{\omega\to 0} -i\omega\hat{\epsilon}(\omega). \tag{2.9}$$

If $c \neq 0$ we know that 0 is a pole of order 1 for $\hat{\epsilon}$. There particular case where $c = 0$ tells us that 0 is not a pole $\hat{\epsilon}$. Therefore if 0 is a pole of ϵ it must be of order 1.
Along with the lack of an imaginary part of $\hat{\epsilon}$ the single pole Drude model only allows complex values of n when $Re(n) = 0$. This would allow for plane waves to not experience any phase shift while traveling through a material. This is a behavior I have not been able to find in the experimental data extracted from [1]

The model does have the merit of having hermitian symmetry. I chose to not try to fit this model on experimental data since it is clearly incapable of modeling it but I will use it in section 2.5 to have a first and simple expression for the reflexion coefficient of a slab.

2.3 Two Pole Drude model

A Different model we can consider is the "two pole Drude model". This one is especially adapted to the study of metals, it assumes that all of the electrons that are contributing to the electric susceptibility are all free electrons. This implies that there is no elastic force acting on them and therefore we can express $\hat{\epsilon}$ as:

$$\hat{\epsilon} = \epsilon_\infty - \frac{\omega_p^2}{\omega^2 + i\gamma\omega} \tag{2.10}$$

We can start by noticing many of the problems we mentioned for the single pole Drude model have been resolved. 0 is a pole of order 1. The model allows for complex values of $\hat{\epsilon}$ even for frequencies on the real axis, all while preserving the hermitian symmetry. By writing (2.10) as a pole expansion, we find that the poles of this expression are 0 and $-i\gamma$ with associated residues of $-\frac{i\omega_p^2}{\gamma}$ and $\frac{i\omega_p^2}{\gamma}$ respectively. It has two poles on the imaginary axis that are in the bottom half of the complex plane. The residues are also imaginary. This shows that this model is coherent with the symmetry properties mentioned in section 1.4.

When fitting a model on complex data it is very difficult to define what is or is not a good fit. For example the measurements of n for gold we obtained from [1] McPeak et al give us $\hat{\epsilon}$ that has an imaginary part that is much smaller than it's real part. Therefore using a curve fitting algorithm like the ones offered by the Python scipy module would try to fit the real part very well without taking into account the imaginary part. With a simple model like the two pole Drude model it is not possible for us to fit both the real and the imaginary part well. So a choice has to be made. I used a fitting method based on a gradient descent algorithm that

uses the python torch module in which i get to define a cost function. This allows me to give more importance to the imaginary part of $\hat{\epsilon}$. I will explain in more detail how the curve fitting program I used functions in A.1.

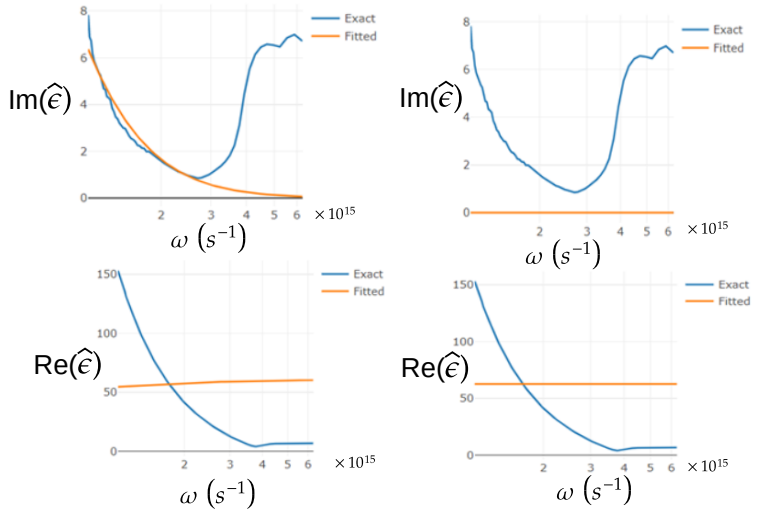

Figure 1: On the left we can compare see how the two pole Drude model approaches experimental data when γ can be negative. On the right we have the same plot but this time γ was set as a positive number. The experimental data displayed in blue coresponds to the mesurements of McPeak et al from [1]and the values obtained after optimisation using the model are in orange.

On figure 1 we can see that this model is not precise enough to take into account the irregular curve that represents $\hat{\epsilon}$ for gold. The same can be found when trying to fit data from different metals. We can notice that on the left graphs the fit seems correspond better on the imaginary part but since the stability of the poles (section 1.4) makes us guarantee that the poles of $\hat{\epsilon}$ are in the bottom half of the complex plane, we can criticise the idea that the left fit is better than the one on the right. On the left figure some poles are on the top half of the complex plane.

We can easily see that in order to find a better model, we need to allow for more variations and different regimes. This can be achieved by adding more poles and in the Drude Lorentz model considering more groups of electrons.

2.4 Drude-Lorentz model

In order to have a model in which we can easily add degrees of liberty while still basing ourselves on (2.6), we can truncate the sum to a limited amount of terms and considering there are free electrons. This can, for example, be expressed as the Drude-Lorentz model as presented by Stout [3]:

$$\epsilon(\omega) = \epsilon_\infty - \frac{\omega_{p0}^2}{\omega^2 + i\gamma_0\omega} - s_1\frac{\omega_{p1}^2}{\omega^2 - \omega_1^2 + i\gamma_1\omega} - s_2\frac{\omega_{p2}^2}{\omega^2 - \omega_2^2 + i\gamma_2\omega} \tag{2.11}$$

Where $\epsilon_\infty \in \mathbb{R}$, $\omega_j \in \mathbb{R}$ and $\gamma_j \in \mathbb{R}_+$ for $j = 0, 1, 2$. By comparing this expression with (2.6) we identify $s_i = \frac{Nn_ie^2}{m\omega_i^2} \in \mathbb{R}_+$. This model gives us more parameters and can be expanded by adding extra Lorentzian terms.

With two Lorentzian terms, the Drude Lorentz model has two poles on the imaginary axis (one of them is 0) and two poles with their conjugates (if p is a pole $-p*$ is a pole). All poles

are of order 1.

In order to fit our data I have given extra liberties to s_i. I allowed it to become negative. This is not coherent with the fact that $s_i = \frac{Nn_ie^2}{m\omega_i^2}$ but that results is a consequence of a very stong hypothesis that the Drude Lorentz Model makes on the behavior of an electron and on the polarisation of matter. Giving this extra freedom to the s coefficients does not contradict any of the properties given by the hermitian symmetry $\hat{\epsilon}$.

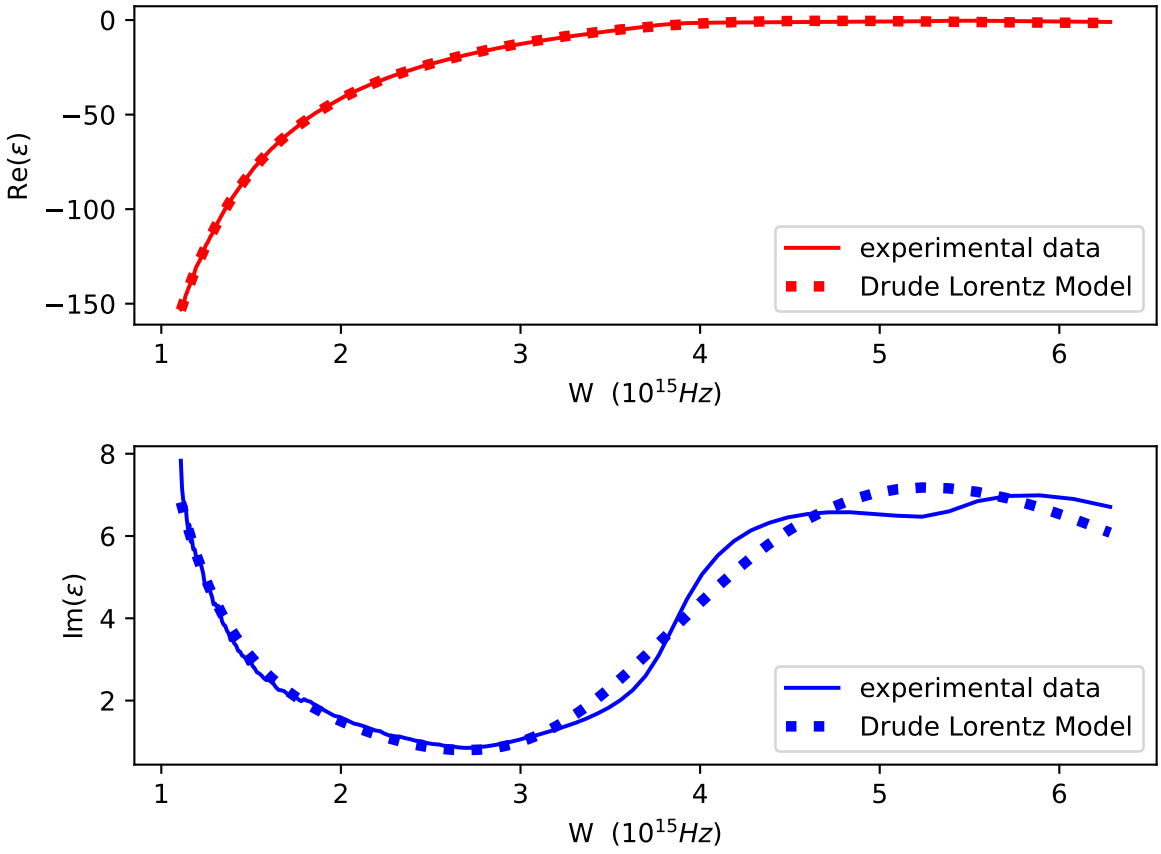

Figure 2: This figure shows the real and imaginary parts of $\hat{\epsilon}$ of gold for real frequencies. The experimental date comes form McPalin et al [1]. The drude Lorentz Model is the one expressed in (2.11). The parameters are:$\epsilon_\infty = 3.997495$, $\omega_{p0} = 14.102417 \times 10^{15} s^{-1}$, $\omega p1 = 5.4614997 \times 10^{15} s^{-1}$, $\omega p2 = 3.5340056 \times 10^{15} s^{-1}$, $\gamma_0 = 0.04383026 \times 10^{15} s^{-1}$, $\gamma_1 = 5.5518894 \times 10^{15} s^{-1}$, $\gamma_2 = 3.1213782 \times 10^{15} s^{-1}$, $s_1 = 8.925666$ and $s_2 = -4.74675$

When looking at figure 2, we immediately see that the Drude-Lorentz Model is able to take into account most of the variations found in the measurements of $\hat{\epsilon}$. By making the cost function in our optimisation algorithm (explained in A.1) give more importance to the Imaginary part without disregarding the importance of the real part the curve we obtain fits the real part of $\hat{\epsilon}$ very well and never gives us an absurd value for the imaginary part. When trying to fit on the imaginary part only the Drude-Lorentz model is unable to achieve results that are better by a significant margin. It simply does not have enough degrees of libeterty to model the final part of the graph of $Im(\hat{\epsilon})$. This figure also shows us that in the visible domain the imaginary part of $\hat{\epsilon}$ is in fact positive. Since this is a condition we imposed on our models in section 1.2 I wanted to check that this condition still held at higher frequencies.

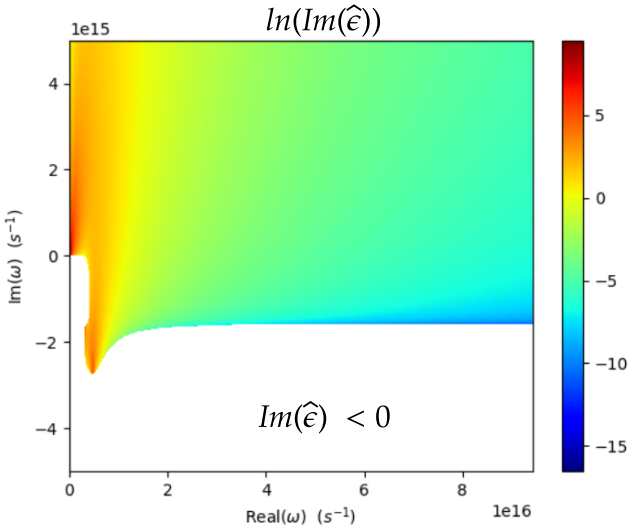

Figure 3: This figure shows the natural log of the imaginary part of $\hat{\epsilon}$ modeled by the Drude-Lorentz with identical parameters as in figure 2. Those parameters correspond to our best fit for the permittivity of gold in the visible domain.

By tracing the logarithm of $Im(\hat{\epsilon})$ on the complex plane while making the area where $Im(\hat{\epsilon}) \leq 0$ white, we can easily see on figure 3 that even for frequencies that far exceed the visible ones on the real axis, the imaginary part of $\hat{\epsilon}$ remains positive. For frequencies with a very low real part the domain on which $Im(\hat{\epsilon}) \leq 0$ comes very close to the real axis but it in fact never reaches the real axis.

In order to futher study (2.11) we will look at it's pole expansion. The first term of (2.11) corresponds to two poles on the imaginary axis with their associated imaginary residues. These correspond to the ones found in the two pole Drude Model, The first non constant term in the Drude-Lorentz Model is associated to a group of free electrons, which is exactly what is modeled in the two Pole Drude Model. In this development, with one or more Lorentzian terms, the poles associated to the term of number n (2.6) are associated to two conjugated poles: $p = \frac{1}{2}(\sqrt{4\omega_n^2 - \gamma_n^2} - i\gamma_n)$ and $-p^* = \frac{1}{2}(-\sqrt{4\omega_n^2 - \gamma_n^2} - i\gamma_n)$. As long as $\gamma_n \geq 0 \quad \forall n$ all the poles of $\hat{\epsilon}$ are stable and the hermitian symmetry is verified. This statement is independent of the amount of terms at which we have truncated (2.6).

This model seems to fit experimental data well, while respecting all properties we chose to impose on $\hat{\epsilon}$. The reason why we still want to use a general pole expansion to model $\hat{\epsilon}$ is because our fitting algorithm was quite inconsistent for finding the correct parameters, it's success was greatly dependent on the initial guess of the parameters. We will also see that using our general pole expansion for $\hat{\epsilon}$ allows us to better model the variation of $\hat{\epsilon}$.

2.5 Comparison between the Drude-Lorentz and the pole expansion Model

In this section we will be discussing the differences and similarities between the Drude-Lorentz model and the one we derived from a pole expansion. For the Drude-Lorentz model we will be using the expression in (2.11). We will therefore be comparing it to a pole expansion with two imaginary poles (among which we will find 0) and 2 poles ouside of the imaginary axis along with their hermitian conjugates.

$$\hat{\epsilon}(\omega) = \epsilon_\infty + \frac{ia}{\omega} + \frac{ib}{\omega + i\gamma_0} + \frac{\alpha_1}{\omega - p_1} - \frac{\alpha_1^*}{\omega + p1^*} + \frac{\alpha_2}{\omega - p_2} - \frac{\alpha_2^*}{\omega + p2^*} \tag{2.12}$$

With $\epsilon_{NR}, \alpha_1, \alpha_2, p_1, p_2 \in \mathbb{C}$ and $\gamma_0, a, b \in \mathbb{R}$.

By grouping the imaginary poles together and the conjugated poles together we can rewrite (2.12) as:

$$\hat{\epsilon}(\omega) = \hat{\epsilon}_\infty + \frac{i\omega(a+b) - a\gamma_0}{\omega^2 + i\gamma_0\omega} + 2\frac{i\omega Im(\alpha_1) + Re(p_1^*\alpha_1)}{\omega^2 - |p_1|^2 + 2i\omega p_1} + 2\frac{i\omega Im(\alpha_2) + Re(p_2^*\alpha_2)}{\omega^2 - |p_2|^2 + 2i\omega Im(p_2)}. \quad (2.13)$$

Which by renaming some variables becomes:

$$\hat{\epsilon}(\omega) = \hat{\epsilon}\infty - \frac{i\omega s_{10}\gamma_0 + \omega_0^2}{\omega^2 + i\gamma_0\omega} - \frac{i\omega s_{11}\gamma_1 + s_{21}\omega_1^2}{\omega^2 - \omega_1^2 + i\omega\gamma_1} - -\frac{i\omega s_{12}\gamma_2 + s_{22}\omega_2^2}{\omega^2 - \omega_2^2 + i\omega\gamma_2}. \quad (2.14)$$

With $s_{10}, s_{11}, s_{12} \in \mathbb{R}$, $\omega_0, \omega_1, \omega_2 \in \mathbb{R}$, $\gamma_0, \gamma_1, \gamma_2 \in \mathbb{R}_+$ and $s_1, s_2 \in \mathbb{R}$.

This expression has more degrees of freedom than the Drude-Lorentz model, To become identical to the Drude-Lorentz model (2.11) we would have to set all the s_{1i} coefficients to 0. This would imply that the residues of the imaginary poles are opposites and that the residues (α_1, α_2) are real. In order to better fit our data we will not try to mimic the expression in (2.11) exactly. The existence of the s_{1k} coefficients which is equivalent to the imaginary part of α_1, α_2 is justified by expressing the $\mathbf{P}$, the polarisation of the medium in the following way.

$$\mathcal{L}_1(\mathbf{P}) = \mathcal{L}_2(\mathbf{E}) \quad (2.15)$$

With $\mathcal{L}_1$ and $\mathcal{L}_2$ linear operators. This expression used in [4] allows $\mathbf{P}$ to be dependant on the derivatives of $\mathbf{E}$. When relating to the way we constructed the Drude-Lorentz model this would justify the appearance of complex residues in the harmonic domain.

We will now be discussing how we were able to fit the data of [1] for different metal using our pole expansion as expressed in 2.12. In section A.1, we presented a cost function L; this function is particularly complicated when fitting 2.14. The same cost function is used when adding extra poles. We wanted to remain close to the solution given by the Drude-Lorentz model because of its success, therefore the cost function has a penalty on the norm of the $s_{1i}gamma_i$ coefficient. If increasing $|s_{1i}\gamma_i|$ does not affect the quality of the fit and the optimisation algorithm will not increase it. This ensures that we remain close to the solutions found by fitting (2.6) if they fit well, while still having extra freedom. Writing $|s_i\gamma_i|$ instead of a single new constant maxes the fact that the formula is homogeneous more apparent and complexifies the variation of $\hat{\epsilon}$ when modifying γ_i. Adding this dependency seem to have helped the convergence of the algorithm, which was a one of the difficulties we had with other models. In the cost function we also identify a penalty when the imaginary part of $\hat{\epsilon}$ is negative. The weight of this penalty had to be balanced keeping in mind the importance of the sign of $Im(\hat{\epsilon})$ while still allowing it to pass through impossible states in order to avoid beeing stuck in a local optimum that does not fit the data wel. Other considerations made on the cost function are of course the error on the real and imaginary parts with corresponding weights so as not to prioritise on more than the other.

Before presenting the set of optimal parameters we have found for different materials, I will express the exact expression we fitted on the data, It is slightly different than 2.14 but counts for any amount of poles on and off the imaginary axis.

$$\hat{\epsilon}(\omega) = \hat{\epsilon}_\infty + i\frac{r_0}{\omega} - \sum_{k=1}^{n} \frac{\omega_{\mathrm{Im}\ k}^2/\Gamma_{\mathrm{Im}k}}{\omega^2 - i|\Gamma_{\mathrm{Im}k}|\omega} - \sum_{k=1}^{m} \frac{i\omega s_{1k}\gamma_k + s_{2k}\omega_{0k}^2}{\omega^2 - \omega_{0k}^2 + i|\gamma_k|\omega}. \quad (2.16)$$

With n and m respectively the number of poles on and outside of the imaginary axis except for 0 which we imposed as a pole of order 0. With all coefficients that are real frequencies exept ϵ_∞ which is without a unit and takes its values in $\mathbb{C}$ and $\omega_{\mathrm{Im}\ k}$ that is real and is expressed in

$s^{-1.5}$. The absolute values have been added in order to ensure all poles remain stable (located in the bottom half of the complex plane). With an identical amount of poles we are able to have a better approximation of experimental data than with the Drude-Lorentz mode. The optimisation algorithm and associated cost function we used for calculating the optimal parameters always converges to a solution while still retaining some randomness in the initial guess. Some initial guesses are done by taking values evenly spaced on a certain domain others others are taken using a function that returns a random number.

I will now be giving the sets of optimal parameters for different metals. There will be 3 non zero poles on the imaginary axis and 5 along with their hermitian conjugates outside of the imaginary axis. This give us a fit that was able to model all significant variation of $\hat{\epsilon}$. This includes the variation the Drude-Lorentz model with 2 Lorentzian terms was unable to acount for on figure 2.

Among the metals that we had data on from [1] we chose to work with the following selection: Au, Ag, Co, TiO2, HfO2, TaO5 and SiO2. We will be focussing on a couple of them to avoid redunduncy.

Results for modeling the curve of gold (Au) from McPalin et al [1]

Table 1: Parameters associated to Poles on the imaginary axis

Pole index	ω_{Im} (Hz)	Γ_{Im} (Hz)
1	5.0740578×10^{10}	1.0000001×10^{10}
2	1.9038134×10^{15}	4.0004995×10^{13}
3	2.9839816×10^{15}	7.9999998×10^{13}

Table 2: Parameters associated to Poles outside of the imaginary axis

Pole index	s_1	s_2	γ (10^{15} Hz)	ω_0 (10^{15}Hz)
1	1.6404576	−1.940789	0.12795785	0.8301875
2	−0.40987584	0.39179462	1.023784	1.8401157
3	−0.00364517	1.6343746	−2.1106775	5.810807
4	2.1277544	1.3592257	−1.2831758	4.2372465
5	−0.00578405	1.7305752	−1.8899007	7.873493

The residual term $\epsilon_\infty = 2.944489$ and $r_0 = -1.6629515 \times 10^{15}$. One could argue that the level of precision of a fit with this many poles could be excessive just as the amount of digits given for any parameter, but since the measurements of refractive index are typically very precise and the data obtained from the database [1] gives us values with precision of 10^{-8} I chose to give every decimal I have access to.

Results for modeling the curve of silver (Ag) from McPalin et al [1]

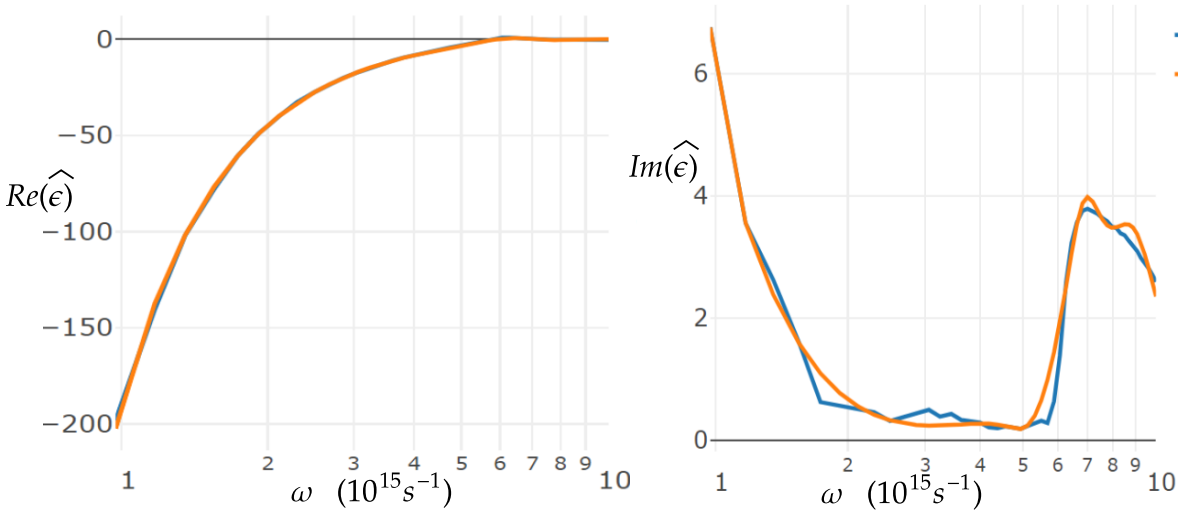

Figure 4: This figure shows exact values of $\hat{\epsilon}$ for silver mesured by McPalin et al [1] in blue and the values predicted by the pole expansion model in orange, for both the real and the imaginary part.

Table 3: Parameters associated to Poles on the imaginary axis

Pole index	ω_{Im} (Hz)	Γ_{Im} (Hz)
1	$-6.1891822 \times 10^{11}$	1.0000001×10^{10}
2	2.1403258×10^{15}	4.0004995×10^{13}
3	2.5494568×10^{15}	7.9999998×10^{13}

Table 4: Parameters associated to Poles outside of the imaginary axis

Pole index	s_1	s_2	γ (10^{15} Hz)	ω_0 (10^{15}Hz)
1	0.10198549	−2.324485	0.5628406	0.96216357
2	−0.6144002	−0.2706777	−2.1505141	4.784233
3	0.00673338	0.9279642	−0.7088824	11.856196
4	−0.01835382	0.6542121	1.5815303	6.864364
5	0.01073925	1.3785194	−3.7010128	8.885926

The residual term $\epsilon_\infty = 0.7533774$ and $r_0 = -1.4046295 \times 10^{15}$. For silver we can often see similar values to the ones obtained for gold. This can be partialy justified by the similarity of the experimental data. Looking at the exact mesurements on figure 2 and 4 the similarities in amplitude and shapes of the curves become evident. This is not true when modeling a metal like Cobalt.

Results for modeling the curve of Cobalt (Co) from McPalin et al [1]

As shown on figure 5 not all metals have a permittivity that behaves similarly to the one of gold and silver. For cobalt the imaginary part of $\hat{\epsilon}$ is often bigger than the real part. Fortunately, the cost function used automatically reajusts the important of each component so that the real and imaginary parts are still as important as each other.

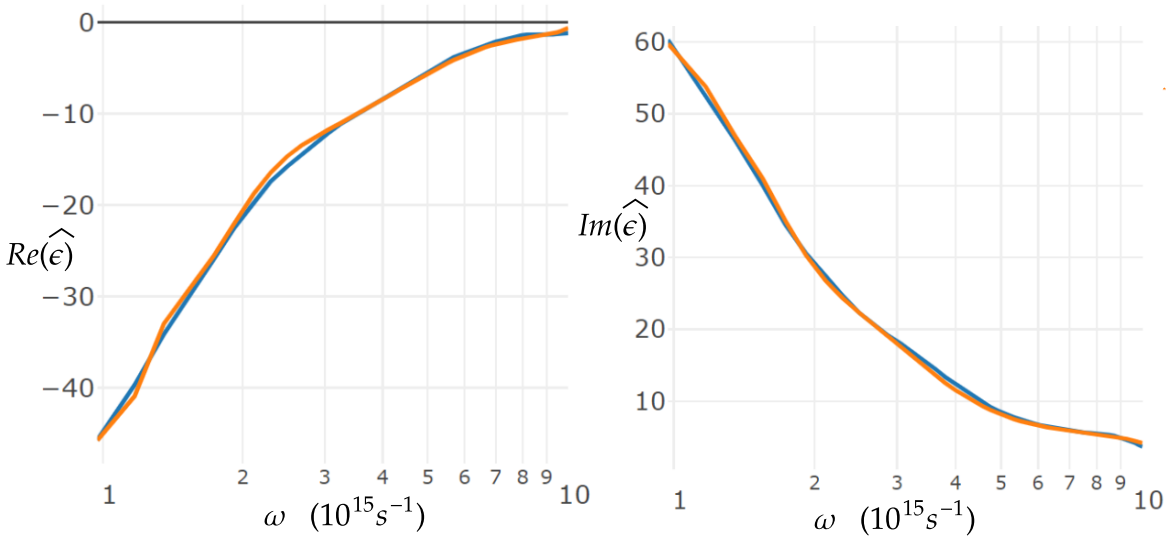

Figure 5: This figure shows exact values of $\hat{\epsilon}$ for cobalt measured by McPalin et al [1] in blue and the values predicted by the pole expansion model in orange, for both the real and the imaginary part.

For cobalt the simpler curve would allow us to use fewer poles in order to model it with satisfying precision but we chose to keep an identical amount of poles in order to be able to compare the values.

Table 5: Parameters associated to Poles on the imaginary axis

Pole index	ω_{Im} (Hz)	Γ_{Im} (Hz)
1	1.8417377×10^{12}	1.0000001×10^{10}
2	1.1628705×10^{15}	4.0004995×10^{13}
3	1.8803284×10^{15}	7.9999998×10^{13}

We can notice that for all the materials we have fitted our model on the Γ_{Im} parameters are identical, this is due to its initialisation which is identical for all materials. Due to the amount of degrees of liberty it is not surprising that some of them did not need to be varied. We can also note that the pole distribution is not necessarily unique given only values of $\hat{\epsilon}$ on the real axis.

Table 6: Parameters associated to Poles outside of the imaginary axis

Pole index	s_1	s_2	γ (10^{15} Hz)	ω_0 (10^{15}Hz)
1	9.0619078	8.199015	$-3.4488991 \times 10^{-1}$	0.9952635
2	-1.1597128	11.573701	9.8283070×10^{-1}	1.440834
3	8.0286694×10^{-1}	2.5359766	5.4270076×10^{-4}	14.035816
4	$-3.6677675 \times 10^{-4}$	12.716653	3.8255720	2.8783154
5	1.7090058×10^{-3}	1.2155031	4.6040025	8.721278

The residual term $\epsilon_\infty = -2.958835$ and $r_0 = 16.066317 \times 10^{15}$.
The example of Cobalt is useful to illustrate the fact that this model can mimic many different curves. The algorithm has a hard time to find parameters that take into account the shapes of curves that only have variation of very small amplitudes. The absolute difference between the measurements and the approximation remains small be it does not have the right shape.

Now that we have a model that seems to model the permittivity of metals well, we can use it to predict the response of a metal slab to incoming waves. The S-matrix of a system gives the outgoing waves when given the incoming waves. We will be looking at one of the reflection coefficients of the S-matrix. First by using simple models for permittivity and then by using our pole expansion model. We will note that since a reflection coefficient corresponds to a physical interaction it does not diverge at infinity (in the time domain) and it is real, therefore it's bilateral Laplace transform has hermitian symmetry. We will be working under the assumption that it does not diverge at infinity in the harmonic domain, therefore the pole expansion we did on $\hat{\epsilon}$ in section 1 can be used on the reflection coefficient, who will also respect all the symmetry properties mentioned for $\hat{\epsilon}$.

2.5.1 The slab and the S-matrix

Let's consider a medium of refractive index n separated from the void by two infinite parallel planes that are separated by a distance d . The index 1 will mean in the void and 2 will mean in the medium. We will call this a slab.

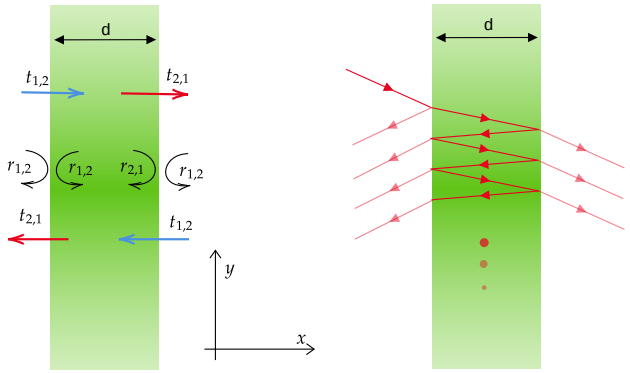

Figure 6: The left figure shows the slab and represents the reflection and transmission coefficients of both interfaces. The right figure shows some of the multiple reflections and transmissions we have to account for in order to calculate the outgoing fields from the incoming fields. The incoming wave should have a normal incidence on the slab. We have represented what happens with a wave that does not have a normal incidence in order to make the multiple reflections more visible.

The S-matrix of a system gives the outgoing signal given the incoming signals, in our case the incoming signals are Electromagnetic waves that propagate towards the slab. We write the S-matrix as follows $S = \begin{pmatrix} \tilde{r_1} & \tilde{t_2} \\ \tilde{t_1} & \tilde{r_2} \end{pmatrix}$. Lets consider the incoming waves are $\vec{E_A}$ from the left and $\vec{E_c}$ from the right and the outgoing waves are $\vec{E_B}$ towards the left and $\vec{E_D}$ towards the right. We assume we are working with plane waves of equal frequency ω and normal incidence on the slab that can be written as $E_X \vec{e_z}$ (we are in the TM convention).

$$\begin{pmatrix} E_B \\ E_D \end{pmatrix} = S \begin{pmatrix} E_A \\ E_C \end{pmatrix} \tag{2.17}$$

. Using the fact that $r_{1,2} = -r_{2,1} = r$ and considering that traveling the distance d induces a phase shift of $\omega \frac{nd}{c} = \omega\tau$ we can find the expressions of E_B and E_C

$$\begin{aligned} E_B &= \left(r - r t_{1,2} t_{2,1} e^{2i\omega\tau} \sum_{k=0}^{\infty} (e^{2i\omega\tau} r^2)^k \right) E_A + t_{1,2} t_{2,1} e^{i\omega\tau} \sum_{k=0}^{\infty} (e^{2i\omega\tau} r^2)^k E_C \\ &= \left(r - \frac{r t_{1,2} t_{2,1} e^{2i\omega\tau}}{1 - r^2 e^{2i\omega\tau}} \right) E_A + \left(\frac{t_{1,2} t_{2,1} e^{i\omega\tau}}{1 - r^2 e^{2i\omega\tau}} \right) E_C \end{aligned} \tag{2.18}$$

$$\begin{aligned} E_D &= \left(r - r t_{1,2} t_{2,1} e^{2i\omega\tau} \sum_{k=0}^{\infty} (e^{2i\omega\tau} r^2)^k \right) E_C + t_{1,2} t_{2,1} e^{i\omega\tau} \sum_{k=0}^{\infty} (e^{2i\omega\tau} r^2)^k E_A \\ &= \left(r - \frac{r t_{1,2} t_{2,1} e^{2i\omega\tau}}{1 - r^2 e^{2i\omega\tau}} \right) E_C + \left(\frac{t_{1,2} t_{2,1} e^{i\omega\tau}}{1 - r^2 e^{2i\omega\tau}} \right) E_A \end{aligned} \tag{2.19}$$

. Therefore we can write $\tilde{r_1} = \tilde{r_2} = \left(r - \frac{r t_{1,2} t_{2,1} e^{2i\omega\tau}}{1 - r^2 e^{2i\omega\tau}} \right)$ and $\tilde{t_1} = \tilde{t_2} = \left(\frac{t_{1,2} t_{2,1} e^{i\omega\tau}}{1 - r^2 e^{2i\omega\tau}} \right)$ The fact that both $\tilde{r_1} = \tilde{r_2}$ and $\tilde{t_1} = \tilde{t_2}$ is due to the fact that on both sides of the slab we have the same refractive index. These results are coherent with the thin layers formalism presented by R.Petit [9].

2.6 Assuming $n(\omega)$ is constant

We will be assuming that n is a constant, then we will derive the singularity expression of $\tilde{r}$, I chose to verify if this simple model still retains the symmetry properties mentioned in section 1.4 and have a closer look a the pole distribution. We can note that since $n = \sqrt{\hat{\epsilon_r}\hat{\mu_r}}$ has a hermitian symmetry, it being a constant implies that n is real.

2.6.1 Poles and residues of $\tilde{r}$

Since the reflection coefficients of the S-matrix are equal we will write $\tilde{r_1} = \tilde{r_2} = \tilde{r}$. The poles $\tilde{r}$ are obtained when $e^{2i\omega\tau} = r^{-2}$.If $p^2 = \frac{1}{r^2}$ we have to solve $e^{2i\omega\tau} = p^2$.

$$e^{2i\omega\tau} = p^2 \implies \omega = -i\frac{ln(p)}{\tau} + \frac{k\pi}{\tau} k \in \mathbb{Z} \tag{2.20}$$

As referenced in section 1.4, since the inverse Laplace transform of $\tilde{r}$ is a real function in the time domain, if ω is a pole of $\tilde{r}$ then $-\omega^*$ is a pole of $\tilde{r}$. By setting $k = 0$ in (2.20) we can deduce that $\left(\frac{iln(p)}{\tau}\right)^*$ is a pole of $\tilde{r}$, therefore the imaginary part of $ln(p)$ must be equal to $\alpha\pi \quad \alpha \in \mathbb{Z}$. Because the complex logarithm of p has the principal argument of p as an imaginary part and we are not considering the sign of p we can assume it is 0. Therefore $r \in \mathbb{R}$ and we have all the poles of $\tilde{r}$. The pole distribution can be verified. Figure 7 verifies that all of our poles have the same imaginary parts and they are regularly spaced.

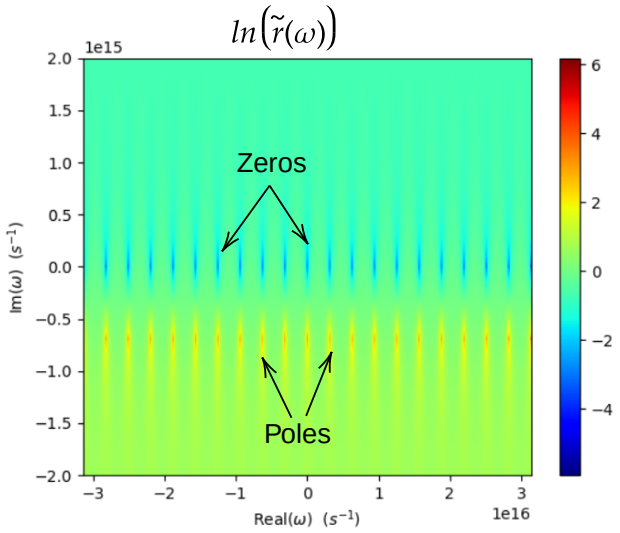

Figure 7: This figure gives the values of $ln(\tilde{r})$ in the complex plane for $n = 3$, $d = 100nm$. We notice the regularly spaced poles and zeros of $\tilde{r}$. The blue points where $ln(\tilde{r})$ tends to $-\infty$ are the zeros and the red points correspond to the poles of $\tilde{r}$.

Now that we have the poles, we need the residues of $\tilde{r}$ as well as the order of the poles. Let's consider $\omega_k = -i\frac{ln(p)}{\tau} + \frac{k\pi}{\tau}$ with $k \in \mathbb{Z}$.

$$\lim_{\omega\to\omega_k}(\omega-\omega_k)\tilde{r(\omega)} = \lim_{\omega\to\omega_k}\left(\frac{(\omega-\omega_k)rt_{1,2}t_{2,1}e^{2i\omega\tau}}{1-r^2e^{2i\omega\tau}}\right) = \lim_{\omega\to\omega_k}\left(-\frac{(\omega-\omega_k)r(1-r^2)e^{2i\omega\tau}}{1-r^2e^{2i\omega\tau}}\right) \quad (2.21)$$

We can use l'Hopital's rule to calculate the previous limit:

$$\lim_{\omega\to\omega_k}(\omega-\omega_k)\tilde{r(\omega)} = \frac{r}{2i\tau}\frac{1-r^2}{r^2} = \frac{1-r^2}{2i\tau r} \quad (2.22)$$

Since that limit exists we know that ω_k is a pole of order 1 and $Res\,(\tilde{r}, \omega_k) = \frac{r}{2i\tau}\frac{1-r^2}{r^2}$.
We can finally give the singularity expansion of $\tilde{r}$ taking into acount that 0 is a zero of $\tilde{r}$

$$\boxed{\tilde{r}(\omega) = \sum_{k=-\infty}^{+\infty}\frac{\tau}{ril n(r) + k\pi}\left(\frac{1-r^2}{2i\tau r}\right) + \sum_{k=-\infty}^{+\infty}\frac{\tau}{\tau\omega - ril n(r) - k\pi}\left(\frac{1-r^2}{2i\tau r}\right)} \quad (2.23)$$

In order to use this pole expansion as an approximation of the function we want to take a limited amount of terms on the previous sum. Previous work on the subject by members of the Clarte research team has shown that using 20 poles is sufficient to have a good approximations of $\tilde{r}$ in the frequency domain [11]. They also found that in the time domain 4 poles are sufficient.

2.7 Assuming n varies with ω

The differences that appear when n becomes dependant on ω are due to the fact that $\tau(= \frac{nd}{c})$ and r are function of n. Since we are in the particular case when the slab is lit under normal incidence we have $r = \frac{n-1}{n+1}$.

In this section we will be comparing the pole and zeros distribution of $\tilde{r}$ for different models of n as well as the coherence of those same models on the example that will be a gold slab.

Gold typically had a very low refraction index. Its modulus is often below 1, which can seem curious since we can often find $n = \frac{c}{v_m}$ with v_m and c respectively the speed of light in the

medium and in the void. Therefore one would expect n to be superior to 1. Since n is not a constant the group velocity and phase velocity of the waves can be different. Furthermore using n to caracterise the velocity of a wave would not make sense since n takes complex values.

Though we can not find a general expression of the poles of $\tilde{r}$ for any model where n varies, we can still calculate it's residues.

Lets consider a pole ω_p we have $\lim_{\omega\to\omega_p} e^{2i\omega\tau} = r^{-2}$. Using $\partial_\omega e^{2i\omega\tau} = 2i\frac{d}{c}\left(n+\omega\partial_\omega n\right)e^{2i\omega\tau}$ we can like in (2.22) apply l'Hopital's rule to find:

$$Res\left(\tilde{r},\omega_p\right) = (r^{-2}-1)\frac{2r}{\frac{2\partial_\omega n}{(n+1)^2}r^{-1} + \frac{id}{c}\left(n+\omega_p\partial_\omega n\right)} \tag{2.24}$$

Before looking at the pole distribution for $\tilde{r}$ when the permittivity is modeled by our pole expansion I will do so with the single pole Drude model. Though it does not reflect reality very well I, thought it was interesting to be able to confront our results with a more simple approach. The hermitian symmetry of $\hat{\epsilon}$ gives us the hermitian symmetry of the pole distribution observed in figure 8.

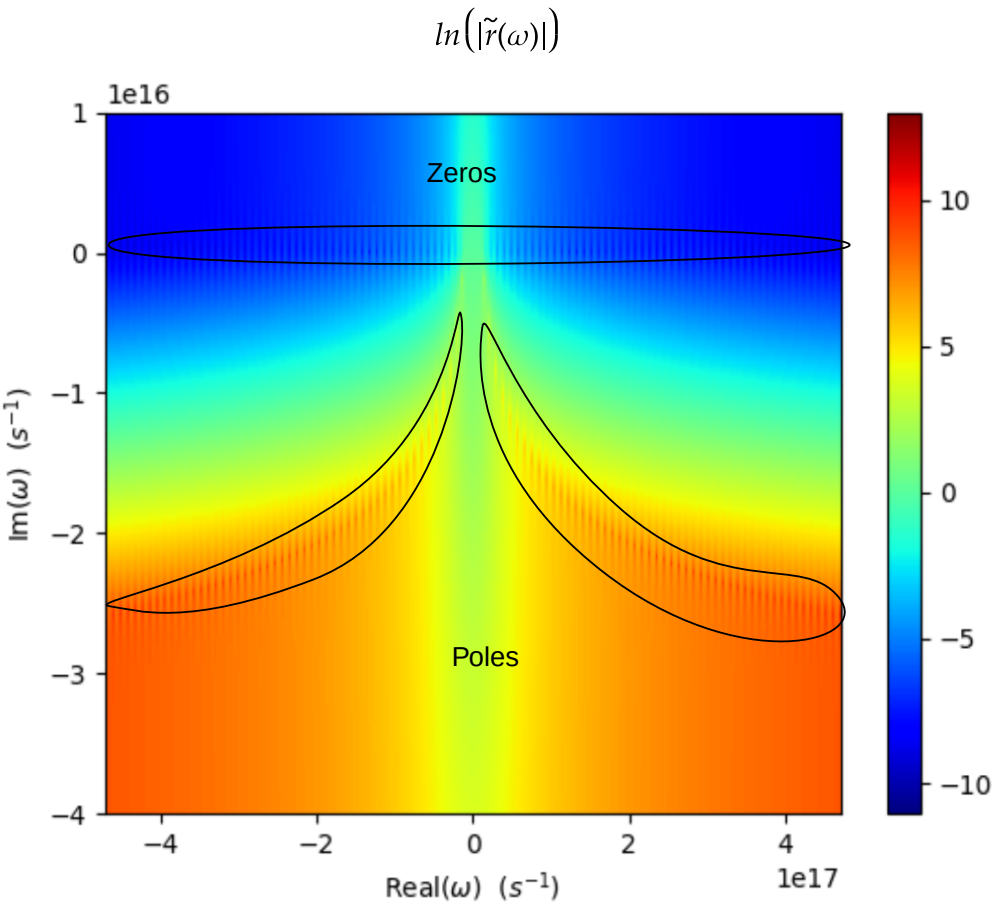

Figure 8: This figure highlights the poles and zeros of $\tilde{r}$, with $\omega_p = 1.26\times10^{16}$ modeled using the single pole Drude model. Since we calculated $\tilde{r}$ on a discrete grid, we have high values at the poles but can never obtain ∞. When closing in on a pole, if we chose to add more points closer to the pole the divergence of the function becomes more evident. This figure verifies the symmetry with respect to the imaginary axis of the pole distribution.

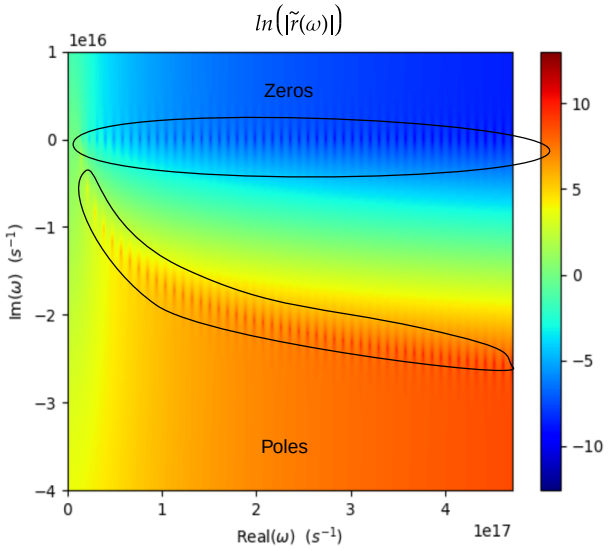

Figure 9: This figure highlights the poles and zeros of $\tilde{r}$, with $\omega_p = 1.26 \times 10^{16}$ modeled using the single pole Drude model

A better look at the evolution of the pole distribution is given in figure 9. Focusing on the right half of the complex plane is justified thanks to the symmetry of $\tilde{r}$. We can see a decrease in the imaginary part of the poles when looking at frequencies where $Re(\omega)$ gets bigger. This decrease is slowing down. Figure 10 shows that when $\omega \to \infty$ the pole distribution becomes the similar to the one observed in figure 7 where n was a constant. Since $\epsilon(\omega)$ converges when $|\omega| \to \infty$. this behavior is as expected. For the reflection coefficient we obtained using the pole expansion method we ofcourse preserved the hermitian symmetry but we do find some more irregular behavior in the pole and zeros distribution. As seen on on figure 11 the evolution of the imaginary part of the poles is not monotone when looking futher from the imaginary axis. In the domain observed on figure 11 the poles fist have their successive imaginary parts that decrease before going up.

On figure 12 we can see that just as we saw with the single pole drude model for very high frequencies we obtain the same behavior as when n is constant. This is of course because with a finite amount of poles for high frequencies $\hat{\epsilon}$ tends to ϵ_∞. The behavior when $Re(\omega) \to \infty$ is found for all the metals we have studied but the other behaviors do differ. We can even see notable differences in the pole distribution of $\tilde{r}$ when switching from gold to silver.

By comparing figure 11 and 13 we see that the reflection coefficient on a silver slab retained a monotone evolution of the imaginary part of the poles which is not true for the gold slab. We could compare all the metals and dielectric materials we have data on and see what behaviors occur but the real important result is that our pole expansion model is able to show different behaviors according to the material it is modeling and that it is very good model for fitting the permittivity of metals and dielectric materials.

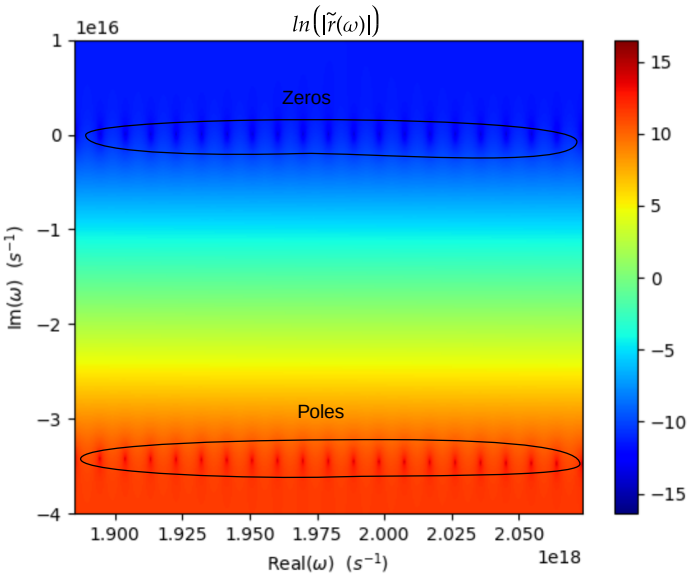

Figure 10: This figure highlights the poles and zeros of $\tilde{r}$, with $\omega_p = 1.26 \times 10^{16}$ for very high frequencies With the single pole Drude model.

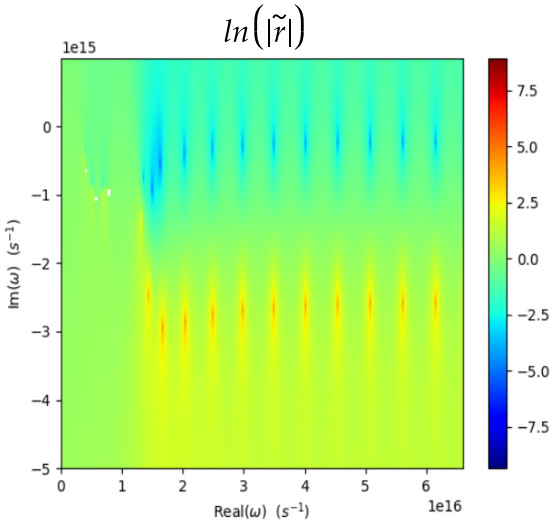

Figure 11: This figure highlights the poles and zeros of $\tilde{r}$, for gold for very high frequencies. Where $\hat{\epsilon}$ is modeled using the pole expansion method and the parameters mentioned in section 2.5

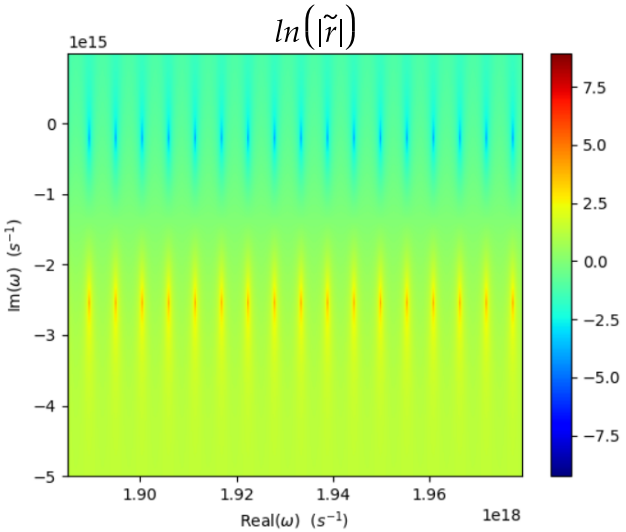

Figure 12: This figure highlights the poles and zeros of $\tilde{r}$, for gold for very high frequencies. Where $\hat{\epsilon}$ is modeled using the pole expansion method and the parameters mentioned in section 2.5. It focusses on a part of the complex plane that is very far from the imaginary axis, it therefore coresponds to very high frequencies.

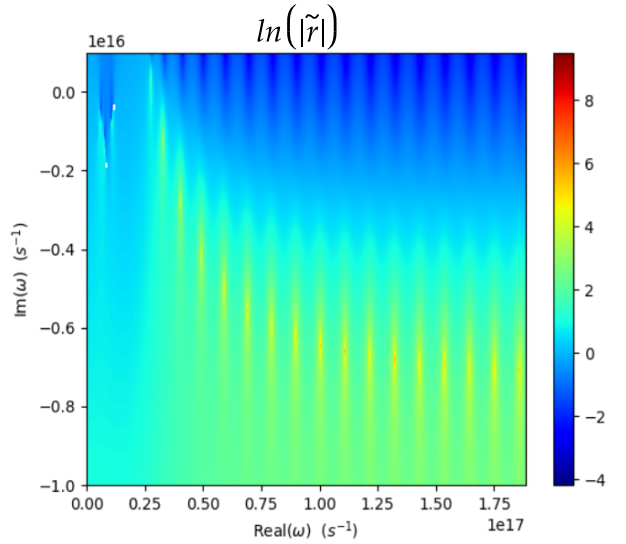

Figure 13: This figure highlights the poles and zeros of $\tilde{r}$, for Silver Where $\hat{\epsilon}$ is modeled using the pole expansion method and the parameters mentioned in section 2.5.

Conclusion and perspectives

We have found that by using a pole expansion to model the permittivity of metals in the time harmonic domain we can model metals very well. Using mathematical properties like the hermitian symmetry of $\hat{\epsilon}$ for example, helped us to find a solution that is coherent with the physical properties of ϵ (Which is real and non divergent). While the amount of poles necessary varies from case to case we had satisfying results by using 0 as a pole along with three other poles on the imaginary axis and 5 outside of the imaginary axis. It has been beneficial for our fitting algorithm to remain close to a model that could be found using the Drude-Lorentz model while simply allowing for a bit more variation. This means that existing studies based on the Drude-Lorentz model could be improved without changing the behavior of the permittivity outside of the real axis by a lot. I was also able to discover how the S-matrix works and study the reflection coefficients of a single layer slab for different materials. Studying the reflection coefficients also thanks to its infinite amount of poles helped me understand some finer properties of pole expansions in general that are discussed by Ben Soltane [10] that I worked on but chose not to talk about in this report due to relevance with the main subject. We can still make many improvements on the pole expansion of the reflexion coefficient of the slab. I only studied the slab with normal incidence and as a single layer linking two identical mediums. This is everything except general and can be generalised by changing the Fresnel coefficients by their angle dependant versions, this is something that a student from Centrale Marseille works on, he will later on be using our model for permittivity. Another path of improvement would be considering with multiple layers of different materials. And finaly a good path of improvement would also be looking at the permittivity of alloys and more complex materials that may for example be meta materials themselves. For my personal conclusion I can say that doing this internship in the Clarte team was a big opportunity and I learned a lot. I was challenged mathematicaly on physics problems in a way I did not expect, while in many classes we do not have the time to verify if we can justify some elemental steps in a calculation (like for example the convergence of an integral) I was encouraged to do so which I enjoyed very much. Tho I did not focus my report on it a big part of my internship was focused on different fitting algorithms, their pros, cons and how they can be implemented. I think that in future projects, internships or even jobs this will be very useful and I think that I can safely way that while a walked in empty handed I left with a lot of new tools and experiences. I was able to discover how to properly use a Fourier or bilateral Laplace transform in physics which is something I had only encountered in Mathematics classes and I also discovered Green functions along with many properties of the dirac distribution but we did not end up using them which is why they are not mentioned in this repport.

A Appendix

A.1 Codes of the Fitting algorithm

The main algorithm used to find the parameters to model the permittivity of a material using our pole expansion is given in this section. We defined a cost function L that is the quantity we want to minimise. Changing how L is calculated affects how the optimisation behaves. Naively one could simple make L return the module of the difference between the model and the experimental data. In our case since for some materials of $\hat{\epsilon}$ the real and the imaginary part are of different magnitudes, using the naive expression of L would not result in great results. It is therefore very important to balance the contributions of the real and imaginary parts of $\hat{\epsilon}$. Physical properties of $\hat{\epsilon}$ like the sign its imaginary part can also be taking into account in L.

Other properties have to be imposed in the way $\hat{\epsilon}$ is calculated. The optimiser (python object that iterates the algorithm) will let the parameters vary freely while retaining their data type. Therefore a float will remain one but if the initial guess is positive it may become negative. This leads to us having to use the absolute value function quite often. In order to allow parameters to become complex when initialised as real floats we need to add $0i$ to them in order to change the data type to complex.

Using the visdom module allows us to visualise in real time how the fit evolves throught the iterations using it was particularly useful to understand the behavior of the algorithm when I started to work on it.

```
import pandas as pd
import numpy as np
import seaborn as sns
import scipy.optimize as sc
import matplotlib.pyplot as plt
from tqdm import trange
from mpl_toolkits.axes_grid1 import make_axes_locatable

import torch
import torch.optim as optim
import visdom

loss_viz = visdom.Visdom()


c = 3e8

def GetRefractiveIndex(ri_file):
    """_summary_  takes the data from the data base
    and converts it to a torch tensors

    Parameters
    ----------
    ri_file : _type_ name of csv file for silver it would be "Ag"

    Returns
    -------
    W : _type_ torch.tensor
        _description_ list of frequencies
    n : _type_ torch.tensor
        _description_ list of values of the optical index
    """

    a = pd.read_csv("BDD/Materiaux/" + ri_file + ".csv")
    sepRealImag = a.index[(a.loc[:,["wl","n"]] == np.array(["wl","k"])).iloc
    [:,0]]
```

```
    csvReal = None
    csvImag = None
    if sepRealImag.shape[0] > 0:
        sepRealImag = sepRealImag[0]
        csvReal = a.iloc[:sepRealImag,:].reset_index(drop=True).to_numpy().
    astype(float)
        csvImag = a.iloc[(sepRealImag+1):,:].reset_index(drop=True).to_numpy().
    astype(float)
    else:
        csvReal = a.to_numpy().astype(float)


    def extend(X):
        return np.unique(X)


    def interpolate(X, M, imag=False):
        Y = np.zeros_like(X)
        for i in range(X.shape[0]):
            x = X[i]
            if x in M[:,0]:
                Y[i] = M[M[:,0]==x,1]
            else:
                id_inf = 0
                id_sup = M.shape[0]-1
                if (M[:,0]<x).sum()>0:
                    id_inf = np.nonzero((M[:,0]<x))[0][-1]
                if (M[:,0]>x).sum()>0:
                    id_sup = np.nonzero((M[:,0]>x))[0][0]

                x_inf, x_sup = M[id_inf,0], M[id_sup,0]
                y_inf, y_sup = M[id_inf,1], M[id_sup,1]
                if x_inf >= x:
                    x_inf = x
                    y_inf = np.exp(-0.1/x) if imag else 1+np.exp(-0.1/x)
                if x_sup < x:
                    x_sup = x
                    y_sup += x

                Y[i] = y_inf + (y_sup - y_inf)/(x_sup - x_inf)*(x - x_inf)
        return Y

    X = csvReal[:,0]
    if not (csvImag is None):
        X = np.hstack([X, csvImag[:,0]]).astype(float)
        X = np.unique(np.sort(X))
    X = extend(X)
    nR = interpolate(X, csvReal)
    nI = np.zeros_like(nR)
    if not (csvImag is None):
        nI = interpolate(X, csvImag, imag=True)

    nR, nI = np.flip(nR).copy(), np.flip(nI).copy()
    n = nR + 1j*nI

    W = np.sort(2 * np.pi * c / (X * 1e-6)) * 1e-15
    nPts = 70
    if W.shape[0] > nPts:
        s = W.shape[0]//nPts
        n = n[0:n.shape[0]:s]
        W = W[0:W.shape[0]:s]
```

```
95
96      return torch.from_numpy(W), torch.from_numpy(n)
97
98
99  def FitMOSEM(W, n, outputFile, nPoles=7, nPolesIm=2, nIter=2500, lr=3.3e-2, q1
    =1., q2=1.):
100     """_summary_ Uses a gradient descent algorithm in order to find
101     optimal parameters to model data using the model derived from the pole
    expansion
102
103     Parameters
104     ----------
105     W :  torch.tensor
106         List of frequencies we have data on
107     n :  torch.tensor
108         mesurements of n for frequencies in W
109     outputFile : string
110                 File name that will be used to save the parameters and
111                 to find the data
112     nPoles : int, optional
113         number of poles not situated on the imaginary axis, by default 7
114     nPolesIm : int, optional
115                number of poles situated on the imaginary axis, by default 2
116     nIter : int, optional
117         Amount of iteration the algorithm will do before stoping and returning
118         the parameters, by default 2500
119     lr : float, optional
120          learning rate used by the opitimiser, by default 3.3e-2
121     q1 : float, optional
122          parameter used to balance the importance of real and imaginary part of
    n, by default 1.
123     q2 : float, optional
124          parameter used to balance the importance of real and imaginary part of
    n, by default 1.
125
126     Returns
127     -------
128     torch.tensor
129     returns all the  parameters found by the gradient descent algorithm
130     """
131
132     scatterColors = np.random.randint(0, 255, (nPoles+nPolesIm+1, 3))
133
134     def H(w, HNR, w0n, s1n, Gn, s2n, w0im, Gim, Gi0):
135         #Calculates values of epsilon_r predicted by the pole expansion model
    given a set of parameters
136         w1 = 0
137         w2 = 0
138         if len(w.shape) == 0:
139             w1 = torch.from_numpy(np.repeat(w, w0n.shape[0])) + 0j
140             w2 = torch.from_numpy(np.repeat(w, w0im.shape[0])) + 0j
141         else:
142             w1 = w[..., None].repeat_interleave(w0n.shape[0], len(w.shape))
143             w2 = w[..., None].repeat_interleave(w0im.shape[0], len(w.shape))
144
145         return 1 + HNR + 1j*Gi0/w - \
146                ((w0im**2/Gim)/(w2**2 + 1j*torch.abs(Gim)*w2)).sum(dim=len(w2.
    shape)-1) - \
147                ((1j*s1n*Gn*w1 + s2n*w0n**2)/((w1**2 - w0n**2) + 1j*torch.abs(Gn)
    *w1)).sum(dim=len(w1.shape)-1)
148
```

```
149
150     def L(HNR, w0n, s1n, Gn, s2n, w0im, Gim, Gi0, n_it):
151         #This is the cost function it returns the quantity that the gradient
    descent algorithm will try to minimise
152         l = torch.zeros(1)
153         Hw = H(W, HNR, w0n, s1n, Gn, s2n, w0im, Gim, Gi0)
154 
155         pI_min = 0.1
156         N = 1000
157 
158         l += 0.005*torch.mean(torch.abs((Hw - n ** 2) ** 2))
159         l += 0.001*torch.mean(torch.abs(torch.sqrt(Hw) - n) ** 2)
160         #The previous contributions corespond to the module of the error on n
    and epsilon
161         A = torch.mean(torch.abs(torch.real((Hw - n ** 2) ** 2)))
162         #A represents the error commited on the real part of epsilon
163         B = torch.mean(q1 * torch.abs(torch.imag((Hw - n ** 2) ** 2)))
164         #B represents the error commited on the imaginary part of epsilon, it is
     balanced with A by q1
165         l += torch.sqrt(A + B)
166         l += 0.1*torch.sum(torch.relu(-np.imag(Hw) + 0.005))
167         # we also represents the fact that epsilon has to a
168         #positive imaginary part.
169         l += 0.03*torch.mean(torch.abs(s1n*Gn))
170         #in order to remain close to the drude loren
171         return l
172 
173     #We initialise all parameters for the initial guess
174     HNR = 0.1*(torch.rand(1) + 2)
175     HNR.requires_grad_(True)
176     w0n = torch.linspace(1e-3, 2*W[-1], nPoles)
177     w0n.requires_grad_(True)
178     s1n = 0.1*(torch.rand(nPoles) + 2)
179     s1n.requires_grad_(True)
180     Gn = 0.01*torch.linspace(1e-3, 8, nPoles)
181     Gn.requires_grad_(True)
182     s2n = 0.1*(torch.rand(nPoles) + 2)
183     s2n.requires_grad_(True)
184     w0im = torch.linspace(1e-3, 8, nPolesIm)
185     w0im.requires_grad_(True)
186     Gim = 0.01 * torch.linspace(1e-3, 8, nPolesIm)
187     Gi0 = torch.tensor([0.01])
188     Gi0.requires_grad_(True)
189 
190     #the optimiser is the one that does the gradient descent algorithm it is
    given all parameters that can be changed
191     optimizer = optim.AdamW([HNR, w0n, s1n, Gn, s2n, w0im, Gim, Gi0], lr=lr)
192     L_array = np.zeros(nIter)
193     i = 0
194     L0 = torch.zeros(1)
195     while i < nIter:
196         #This loop is the execution of the gradient descent algorithm one
    iteration at a time
197         optimizer.zero_grad()
198 
199         Ln = L(HNR, w0n, s1n, Gn, s2n, w0im, Gim, Gi0, i)
200         dL = (Ln - L0).detach().numpy()
201         L_array[i] = Ln.detach().numpy()
202         if not (np.isnan(dL)):
203             L0 = Ln
204 
```

```
            Ln.backward()
            optimizer.step()

            i+=1

            vizDict = dict(xlabel="iteration",
                           ylabel="loss",
                           title="Cout (" + rf_file + ")",
                           ytype="log")
            loss_viz.line(X=np.arange(i),
                          Y=L_array[:i],
                          opts=vizDict,
                          win="cost")


            if (i%20) == 0:
            # every 20 iterations the values of epsilon are sent to a visual interface called visdom
                Hw = H(W, HNR, w0n, s1n, Gn, s2n, w0im, Gim, Gi0).detach().numpy()

                # REAL, IMAG, ABS CURVES
                Y0 = torch.real(n**2)
                Y1 = np.real(Hw)
                y = np.vstack([Y0, Y1])
                x = np.vstack([W, W])
                vizDict = dict(xlabel="frequence",
                               ylabel="H",
                               title="real",
                               xtype="log",
                               legend=["Exact", "Fitted"])
                loss_viz.line(X=x.transpose(),
                              Y=y.transpose(),
                              opts=vizDict,
                              win="curves_real")

                Y0 = torch.imag(n**2)
                Y1 = np.imag(Hw)
                y = np.vstack([Y0, Y1])
                x = np.vstack([W, W])
                vizDict = dict(xlabel="frequence",
                               ylabel="H",
                               title="imag",
                               xtype="log",
                               legend=["Exact", "Fitted"])
                loss_viz.line(X=x.transpose(),
                              Y=y.transpose(),
                              opts=vizDict,
                              win="curves_imag")

                Y0 = torch.abs(n**2)
                Y1 = np.abs(Hw)
                y = np.vstack([Y0, Y1])
                x = np.vstack([W, W])

                vizDict = dict(xlabel="frequence",
                               ylabel="H",
                               title="abs",
                               xtype="log",
                               legend=["Exact", "Fitted"])
                loss_viz.line(X=x.transpose(),
```

```
                                Y=y.transpose(),
                                opts=vizDict,
                                win="curves_abs")
            else:
                print("ERREUR")
                break
        #the next comand saves the parameters in the .npy format
        np.save("BDD/Materiaux/MOSEM/" + outputFile + "_HNR.npy", HNR.detach().numpy
        ())
        np.save("BDD/Materiaux/MOSEM/" + outputFile + "_w0n.npy", w0n.detach().numpy
        ())
        np.save("BDD/Materiaux/MOSEM/" + outputFile + "_s1n.npy", s1n.detach().numpy
        ())
        np.save("BDD/Materiaux/MOSEM/" + outputFile + "_Gn.npy", Gn.detach().numpy()
        )
        np.save("BDD/Materiaux/MOSEM/" + outputFile + "_s2n.npy", s2n.detach().numpy
        ())
        np.save("BDD/Materiaux/MOSEM/" + outputFile + "_w0im.npy", w0im.detach().
        numpy())
        np.save("BDD/Materiaux/MOSEM/" + outputFile + "_Gim.npy", Gim.detach().numpy
        ())
        np.save("BDD/Materiaux/MOSEM/" + outputFile + "_Gi0.npy", Gi0.detach().numpy
        ())

        return HNR.detach().numpy(), w0n.detach().numpy(), s1n.detach().numpy(), Gn.
        detach().numpy(), s2n.detach().numpy(), w0im.detach().numpy(), Gim.detach().
        numpy(), Gi0.detach().numpy()

n_files = [ "Au2", "TiO2", "SiO2", "HfO2", "Co", "Ag", "Co", "Ta2O5"]
outputObj = []
for rf_file in n_files:
    W, n = GetRefractiveIndex(rf_file)
    nR = torch.real(n)
    nI = torch.imag(n)
    q1 = torch.abs(torch.real(n ** 2)) / torch.abs(torch.imag(n ** 2))
    q1[torch.abs(torch.imag(n ** 2)) < 1e-1] = 1
    q2 = torch.abs(nR) / torch.max(torch.abs(nI))
    q2[torch.abs(torch.imag(n)) < 1e-1] = 1
    q1[q1 <0.4] = 1
    q2[q2 <0.4] = 1

    outputObj.append(FitMOSEM(W, n, rf_file, nPoles=5, nPolesIm=3, nIter=10000,
    lr=0.05, q1=q1, q2=q2))
```

References

[1] Refractive index database. URL:https://www.refractiveindex.info.

[2] Smith D Y et al. A generalized cauchy dispersion formula and the refractivity of elemental semiconductors. *Journal of Physics: Condensed Matter*, 2001.

[3] Stout.B et al. Spectral expansions of open and dispersive optical systems: Gaussian regularization and convergence. *New Journal of Physics*, 2021.

[4] M. Garcia-Vergara, G. Demésy, and F. Zolla. Extracting an accurate model for permittivity from experimental data: hunting complex poles from the real line. *Opt. Lett.*, 42(6):1145–1148, Mar 2017.

[5] Victor Grigoriev, Guillaume Demésy, Jérôme Wenger, and Nicolas Bonod. Singular analysis to homogenize planar metamaterials as nonlocal effective media. *Phys. Rev. B*, 89:245102, Jun 2014.

[6] David Jackson.J. *Électrodynamique classique*. Dunod, 2010.

[7] E. A. Muljarov and W. Langbein. Resonant-state expansion of dispersive open optical systems: Creating gold from sand. *Phys. Rev. B*, 93:075417, Feb 2016.

[8] Kurt E. Oughstun and Natalie A. Cartwright. On the lorentz-lorenz formula and the lorentz model of dielectric dispersion. *Opt. Express*, 11(13):1541–1546, Jun 2003.

[9] Roger P. *Ondes électromagnétiques en radioélectricité et en optique*. Masson, 1989.

[10] I.Ben Soltane, Rémi Colom, **Félice Dierick**, Brian Stout, and Nicolas Bonod. Multiple-order singularity expansion method. *submitted for review*.

[11] Ben Soltane.I, Colom.R, Stout.B, and Bonod.N. Derivation of the transient and steady optical states from the poles of the s-matrix. *Laser and photonics review*, 2022.

Abstract

In this report we derive a Pole expansion for permittivity. In doing this we discuss different properties of the electric permittivity in the time harmonic domain. This model is then in section 2 compared to existing models and to experimental data that came from measurements of the optical index n. Finally in the last section, we use the existing models for permittivity, as well as the model derived thanks to a pole expansion, to calculate the response of a slab to a plane wave. We then discus the pole distribution of the reflection coefficient of the slab.

Keywords: Poles expansion, slab, electromagnetism, permittivity, meta-materials